IEEE Access
Multidisciplinary · Rapid Review · Open Access Journal

Fault-Locator Scheme for Combined Taba-Aqaba transmission system Based on New Faulted Segment Identification Method

M. A. Elsadd[1], Hala A. Omar[2], Ahmed R. Adly[3], and Ahmed F. Zobaa[4,*]

[1]Electrical Engineering Department, Faculty of Engineering, Damanhour University, Egypt.
[2]Basic Engineering Science Department, Faculty of Engineering, Menoufia University, Egypt.
[3]Nuclear Research Center, Egyptian Atomic Energy Authority, Egyptian Atomic Energy Authority, Cairo, Egypt
[4]Electronic and Electrical Engineering Department, Brunel University London, Uxbridge, United Kingdom

* Corresponding author: azobaa@ieee.org

Abstract—In this paper, a new fault locator scheme is introduced to address the non-homogeneity of combined transmission lines (Taba-Aqaba Intertie transmission system). To achieve this goal, the faulted side is first determined using a new algorithm for identifying faulted segments. This identification algorithm relies on the voltage's rate of change along the nonhomogeneous lines in the pure positive-sequence circuit, exploiting the inequality of positive-sequence impedances between power cables and overhead lines. The number of outputs generated by the algorithm is one less than the number of line segments being analyzed. For systems with two segments, the output directly identifies the faulted segment. However, for combined lines with three segments, a new voting system is utilized to determine the faulted segment. The fault distance is then calculated based on the identified faulted segment. To evaluate the proposed scheme, various fault scenarios are simulated on the Taba-Aqaba Intertie transmission system, which connects the Egyptian and Jordanian networks, using ATP-EMTP. These tests encompass different fault types and locations, including cases near the interconnection points between the segments. Additionally, the scheme is tested under nonlinear faults.

Indexes- Fault location; Combined transmission lines; Submarine cable; ATP; Positive-sequence impedance; Symmetrical components.

I. INTRODUCTION

Electrical power is typically transmitted from power stations to substations near loads through overhead transmission lines. However, due to environmental requirements, modern construction often utilizes underground cables for power transfer. Additionally, power is transferred between countries through DC or AC submarine cables. As a result, combined power cables with overhead transmission lines are created [1-2]. The characteristics of overhead lines differ significantly from those of power cables. The cable's impedance is low due to the small space between the conductors. However, the cable capacitance is greater than that of overhead lines due to higher dielectric constants of the insulation materials used and the shorter distance between the sheath and the cable conductors. Consequently, the cable surge impedance is approximately 10% of that of an overhead line (ranging from 40 to 60 Ω for underground cables and 400 to 600 Ω for overhead lines) [2]. Transmission systems are prone to various fault occurrences, with both overhead lines and power cables being susceptible to shunt faults [3]. Therefore, a variety of protective devices are employed to detect and isolate faults on the transmission lines. Moreover, accurately determining the fault location is crucial for quickly initiating the necessary repair processes and reducing costs [4-5].

Fault-distance estimation for combined lines presents a challenge due to the unequal impedances per unit length of the cable and the overhead line. Fault locator algorithms based on artificial neural networks require higher training effort compared to conventional methods to mitigate the potential interference that can lead to erroneous identification of the faulted section. On the other hand, traveling wave-based fault locator algorithms necessitate a single value for the propagation velocity. The fundamental phasor components- based fault locator algorithms typically require a single value for both positive- and zero- sequence line impedances. Additionally, the problem becomes more complex when the combined transmission system contains three different segments, such as the actual transmission line connecting the Egyptian and Jordan electricity networks.

The application of artificial neural network for fault distance estimation in combined transmission line is introduced in [6]-[8]. These approaches typically involve two stages. In the first stage, the faulted side is determined whereas in the second stage, the fault distance is estimated. In [6], the support vector machine is employed to identify the faulted section. In [7], an adaptive network-based fuzzy inference system (ANFIS) with four inputs is employed for the training process to locate the fault. In [8], a new scheme that can detect, classify, and locate the faults for two- and multi-terminal transmission lines is proposed. This scheme is based on the fast-discrete orthogonal S-transform (FDOST) in conjunction with the support vector machine (SVM). The signals of the three-phase currents are measured at a line end to obtain the entropy of FDOST coefficients, and then these coefficients are fed to support vector regression (SVR) to detect the fault location. However, in [6]-[8], the retraining process is again required when significant changes occur in the system configuration.

Travelling waves are utilized to locate faults in combined transmission lines, as described in [9]. However, this method requires a high sampling frequency. Dynamic load conditions,

1

IEEE *Access*
Multidisciplinary : Rapid Review : Open Access Journal

Nomenclature

		γ_{OH1}	the propagation constant of overhead line within positive-sequence circuit
x_{jun}	the fault-side indicator	Zc_{OH_1}	the positive-sequence characteristic impedance of overhead line
L_C	the cable length	x_{jun1}	the calculated distance by considering an artificial fault at the first junction point jun1
L	the total combined line length	x_{jun2}	the calculated distance by considering an artificial fault at the second junction point jun2
ΔV_{jun1}	the positive-sequence voltage change value of the junction point	ΔV_{jun2_1}	the positive-sequence voltage change value of jun2
ΔV_{SA1}	the positive-sequence voltage change value of Busbar A	ΔI_{jun2_1}	the positive-sequence current change value of jun2
ΔV_{SB1}	the positive-sequence voltage change value of Busbar B	L_{OH1}	the length of first overhead line section
ΔI_{A1}	the positive-sequence current change value of Busbar A	L_{OH2}	the length of second overhead line section
ΔI_{B1}	the positive-sequence current change value of Busbar B	ΔV_{jun1_1}	the positive-sequence voltage change value of jun1
Z_{C1}	the cable positive-sequence impedance per unit length	ΔI_{jun1_1}	the positive-sequence current change value of jun1
Z_{OH1}	the overhead positive-sequence impedance per unit length	$A_{OH1}, B_{OH1}, C_{OH1}$, and D_{OH1}	the constants of overhead line connected to busbar A considering the distributed line model
x_{act}	the actual distance	**List of abbreviations**	
ΔV_{f1}	the positive-sequence voltage change value of fault point	ANFIS	adaptive network-based fuzzy inference system
$A_{OH2}, B_{OH2}, C_{OH2}$, and D_{OH2}	the constants of overhead line connected to busbar B considering the distributed line model	FDOST	fast-discrete orthogonal S-transform
γ_{c1}	the propagation constant of cable within positive-sequence circuit	SVM	support vector machine
Zc_{c_1}	the positive-sequence characteristic impedance of cable	SVR	support vector regression

such as abrupt connections of industrial loads, affect fault current levels in a power system. Load increases lead to higher fault currents, while load decreases result in reduced fault currents. Considering dynamic loading's influence is critical in power system design, including protective scheme development, current transformer selection, and choosing protective devices, to ensure safe fault handling and prevent equipment damage [10]. The dynamic loading affects fault location techniques based on traveling waves. Fluctuations in transmission line impedance due to dynamic loading affect the reflection and transmission of fault-generated transient signals [10], making accurate fault location estimation challenging in the time domain. Additionally, dynamic loading causes variations in the line charging current [10], influenced by line capacitance and length, which can interfere with transient signal detection and interpretation, potentially complicating the fault location process. On the other hand, the dynamic loading affects the accuracy of fault location techniques based on the fundamental phasor components using single-end measurements by introducing uncertainties in the estimation of fault resistance, crucial for the accuracy of these techniques. This negative effect can be mitigated through accurate load modeling, which aids in predicting the dynamic behavior of the system and enables more precise fault location estimation.

Additionally, fault location techniques using Phasor Measurement Units (PMUs), which are devices that measure the phasors of voltage and current at high-speed, provide synchronized real-time data from various locations in the power system. By using PMU data, the impact of dynamic loading on the fundamental phasor components- based fault location using two-end measurements can be minimized since the measurements remain unaffected by data latency.

The fault location determination by utilizing the fundamental phasor components is introduced in [11]-[14]. In [11] and [12], the fault location for cascaded overhead cable transmission line is obtained by equating the voltage equation at fault point as a function of measured electrical quantities at one terminal and quantities at the junction point computed from another terminal using modal components based on DFT. This approach yields two solutions: The correct solution is less than the considered faulted section length whereas the improper solution is more than the considered healthy section length. This idea is further developed in [13] to be applicable to two-terminal multi-section nonhomogeneous transmission lines using synchronized phasor measurements. In this case, a selector is introduced to discriminate the faulted zone, and then fault distance estimation can be performed. The authors in [13] extend their work to three-terminal nonhomogeneous transmission lines by

2

introducing an indicator that identifies both the faulted branch and the specific zone (cable/overhead) within the branch, as demonstrated in [14]. Additionally, [15] presents a technique consisting of two steps: the first step involves converting the system of nonlinear equations into an optimization problem, and the second step involves solving the problem using a modified Newton method.

A technique based on prior morphological spectrum and forward and backward traveling waves, suitable for nonhomogeneous distribution systems using measurements at one end, is proposed in [16]. Similarly, a work locating a fault on combined transmission lines (an overhead line combined with an underground cable) by extracting the traveling wave arrival times of the measured voltages using two consecutive sliding windows and curve fitting is developed in [17]. Both [16] and [17] require a high sampling frequency for accurate results. It is important to note that traveling wave-based techniques necessitate substantial computational burden and specially designed transducers. To introduce an additional faulted section identifier independent of the fault location calculations, a new approach in this paper is presented concentrating on an actual combined transmission line connecting between Egyptian and Jordan electricity networks (Taba-Aqaba Inter–Tie transmission system).

The primary objective of this paper is to introduce a novel faulted-section identification scheme for a practical transmission system consisting of overhead lines, submarine cables, and overhead lines, specifically the Taba-Aqaba Inter-Tie transmission system. Importantly, the calculation process of the presented identification method is independent of fault distance calculations. The output of this faulted segment indicator directly indicates the faulted segment when the transmission line has two segments. However, in the case of the Taba-Aqaba Inter-Tie transmission system with three different segments, the identification method produces two outputs. To determine the faulted segment, a comparator or voting system is employed. Subsequently, the fault location is computed based on the identified faulted segment. Notably, the presented scheme is robust against variations in source impedance, fault type, and zero-sequence circuit parameters, making it applicable for submarine cables. To validate the reliability of the scheme, extensive simulation cases were conducted using ATP-EMTP. The results demonstrate that the proposed identification method is reliable under various fault conditions.

II. Introduced Fault-locator Algorithm for Combined Transmission Lines

The non-homogeneity of the combined transmission lines poses a problem for both single- and two-ended fault location techniques. In one-ended techniques, the issue arises from the changing positive-sequence impedance per unit length, which is a crucial input for algorithms, depending on the fault location. As a result, the accuracy of conventional algorithms varies significantly with changes in the fault distance. In two-terminal techniques, the challenge lies in identifying the faulted side of the transmission line. This paper introduces a new algorithm for identifying the faulted side in two-terminal combined lines with three different segments, such as the Taba-Aqaba Inter-Tie

transmission system. The introduced identification method is initially demonstrated using a cascaded overhead-cable transmission line with only two segments.

A. Faulted segment identification

A1. Combined line having two segments

A transmission line, shown in Fig. 1, consists of an underground cable combined with an overhead line. At the junction point, a shunt fault occurs. This combined transmission line connects two substations, A and B. To locate the fault on the combined line, the faulted side must be determined first, and then the fault location is computed. In other words, for faults on either the cable or overhead line segment, the difficulty arises from the presence of an unknown length on this segment, which has a different rate of voltage change compared to the cascaded nonhomogeneous segment. Fig. 2 provides an illustration of this scenario.
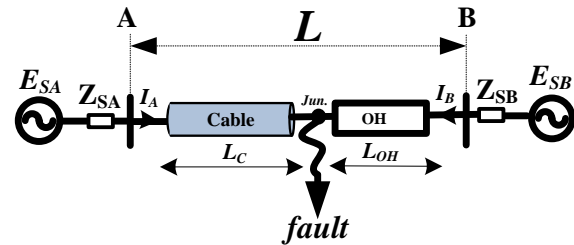

FIGURE 1. A cascaded overhead transmission line with cable connections, experiencing a fault at the junction point.

The identification of the faulted side is accomplished by introducing a formula for identifying the faulted side (x_{jun}). The fault-side indicator (x_{jun}) is a calculated distance under considering an artificial fault at the junction point regardless of the actual fault point. This obtained distance (x_{jun}) precisely identifies the faulted side whether the fault is on the cable or overhead side. If x_{jun} is less than the cable length (L_C) then the fault must be on the cable section and vice versa. This is illustrated in detail as follows:

The fundamental concept behind the fault-side indicator (x_{jun}) is illustrated in Fig. 2, where the capacitor current is neglected to simplify the illustration. This allows for a linear representation of the voltage magnitude variation along the length of each segment of the combined line. The formula of x_{jun} is derived by equating the formulas of the change in positive-sequence voltage at the junction point (ΔV_{jun1}) from both ends of the combined line using the short model representation, irrespective of the actual fault position as shown in (1).

$$x_{jun} = \frac{\Delta V_{SA1} - \Delta V_{SB1} + L \cdot Z_{OH1} \cdot \Delta I_{B1}}{Z_{OH1} \cdot \Delta I_{B1} + Z_{C1} \cdot \Delta I_{A1}} \tag{1}$$

where, ΔV_{SA1} and ΔV_{SB1} represent the changes in positive-sequence voltage components at Busbars A and B, respectively. ΔI_{A1} and ΔI_{B1} represent the changes in positive-sequence current components at Busbars A and B, respectively. The positive sequence components are chosen to be suitable for all types of faults, while the change values are used to mitigate the impact of the capacitive charging current and pre-fault current. These

3

components are estimated using the measured three-phase voltages and currents. x_{jun} is the fault-side indicator. Z_{C1} and Z_{OH1} represent the positive-sequence impedances per unit length of cable and overhead line, respectively. These parameters are known, and their values remain unchanged regardless of the fault point. L denotes the total combined line length, which is equal to the sum of cable length (L_C) and overhead line length (L_{OH}) as depicted in Figs. 1 and 2.
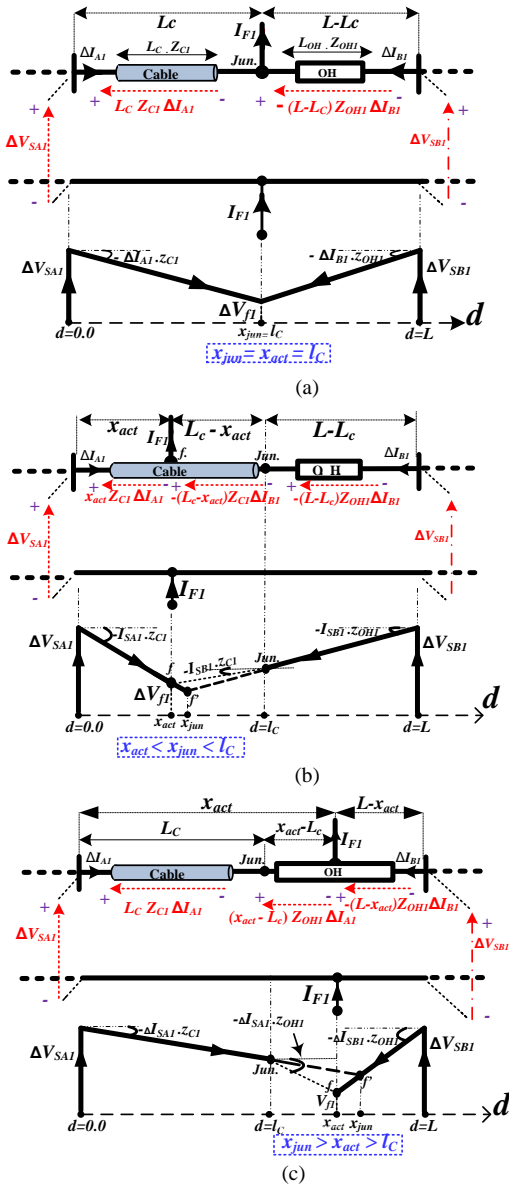

in Figs. 2.a, 2.b, and 2.c respectively - is expressed as (2), (3), or (4) respectively.

$$\Delta V_{SA1} - \Delta V_{SB1} = L_c \cdot Z_{C1} \cdot \Delta I_{A1} - (L - L_c) \cdot Z_{OH1} \cdot \Delta I_{B1} \quad (2)$$

$$\Delta V_{SA1} - \Delta V_{SB1} = x_{act} \cdot Z_{C1} \cdot \Delta I_{A1} - (L_c - x_{act}) \cdot Z_{C1} \cdot \Delta I_{B1} - (L - L_c) \cdot Z_{OH1} \cdot \Delta I_{B1} \quad (3)$$

$$\Delta V_{SA1} - \Delta V_{SB1} = L_c \cdot Z_{C1} \cdot \Delta I_{A1} + (x_{act} - L_c) \cdot Z_{OH1} \cdot \Delta I_{A1} - (L - x_{act}) \cdot Z_{OH1} \cdot \Delta I_{B1} \quad (4)$$

Then, the output of the introduced formula of x_{jun} is expected to be as shown in (5), (6), and (7) by substituting (2), (3), and (4) into (1) and performing some mathematical simplifications for a fault at junction point, cable side, and overhead side, respectively.

$$x_{jun} = x_{act} = L_c \quad (5)$$

$$x_{jun} = x_{act} + (L_c - x_{act}) \cdot \frac{Z_{OH1} \cdot \Delta I_{B1} - Z_{C1} \cdot \Delta I_{B1}}{Z_{OH1} \cdot \Delta I_{B1} + Z_{C1} \cdot \Delta I_{A1}} \quad (6)$$

$$x_{jun} = x_{act} + (x_{act} - L_c) \cdot \frac{Z_{OH1} \cdot \Delta I_{A1} - Z_{C1} \cdot \Delta I_{A1}}{Z_{OH1} \cdot \Delta I_{B1} + Z_{C1} \cdot \Delta I_{A1}} \quad (7)$$

One can observe the following points. Under faults at junction point, the obtained fault distance equals the actual fault distance, as shown in (5). under cable side faults, assuming that the rate of change of the selected voltage component through the unknown cable partition length (L_c-x_{act}) equals $Z_{OH1}.\Delta I_{B1}$ instead of the actual value $Z_{C1}.\Delta I_{B1}$, the actual fault distance (x_{act}) is less than the obtained output value of x_{jun} by a correction factor. This factor is directly proportional to the difference between the actual and assumed rates of change of the considered voltage component, expressed as a ratio of the sum of the two actual rates of change, as shown in (6). This factor is less than 1. Therefore, if the fault is on cable side, x_{jun} must be more than the actual distance (x_{act}), but it must also be less than the cable length (L_C). This is further supported by the voltage magnitude profile of the pure positive-sequence circuit depicted in Fig. 2.b, where the Z_{OH1} is higher than the Z_{C1}. The decreasing rate of the selected voltage component in the region between the junction and fault points, illustrated by dashed line in Fig. 2.b, is higher than the actual decreasing rate depicted by dotted line. Consequently, the calculated positive-sequence voltage reaches the intersection point at a distance (x_{jun}) that is more than x_{act}. However, x_{jun} is less than L_C because the voltage calculation from the direction of Busbar B is accurate until the junction point. Therefore, the value of ΔV_{jun1} calculated from this direction is more than the actual value of the change in positive-sequence voltage at the fault point ΔV_{f1}, as illustrated in Fig. 2.b.

Similarly, in the case of overhead side faults, assuming that the rate of change of the voltage through the unknown overhead partition length (x_{act}-L_c) equals $Z_{C1}.\Delta I_{A1}$ instead of the actual value $Z_{OH1}.\Delta I_{A1}$, the actual fault distance (x_{act}) is less than the obtained output value of x_{jun} by a similar correction term as shown in (7). Thus, if the fault is on overhead side, x_{jun} must be more than x_{act} and then more than L_C. This is further supported

FIGURE 2. The pure positive-sequence circuit and its voltage magnitude profile to investigate the x_{jun} value under a fault at: (a) the junction point (b) the cable side (c) the overhead side.

This obtained distance (x_{jun}) accurately identifies the faulted side whether the fault is on the cable or overhead side. This is proved as follows: The evidence supporting the authenticity of the introduced indicator (x_{jun}) is demonstrated by substituting with the actual difference between the changes in positive-sequence voltages at terminals A and B due to the occurrence of a fault (ΔV_{SA1} - ΔV_{SB1}) as in (1). This voltage difference (ΔV_{SA1} - ΔV_{SB1}) under the three possible fault conditions - a fault at the junction point, cable side, or overhead side, as illustrated

by the voltage magnitude profile shown in Fig. 2.c where Z_{C1} is lower than Z_{OH1}. The decreasing rate of the calculated positive-sequence voltage in the region between the junction and fault points, illustrated by the dashed line in Fig. 2.c, is lower than the actual decreasing illustrated by the dotted line. Consequently, the positive-sequence voltage calculated from the direction of Busbar A reaches the intersection point at a distance (x_{jun}) that is more than x_{act}. Finally, the obtained value of the x_{jun} successfully identifies the faulted section for combined lines with two segments. However, the capacitive charging current should be taken into consideration.

To account for the effect of capacitive charging current, the formula is derived by equating the calculated change in positive-sequence voltage at the junction point (V_{jun1}) from both ends of the combined line, using the distributed line model representation regardless of the actual fault location, as shown in (8).

$$\Delta V_{SA1} \cosh(\gamma_{c1} x_{jun}) - \Delta I_{A1} Zc_{c_1} \sinh(\gamma_{c1} x_{jun}) = \Delta V_{SB1} \cosh(\gamma_{OH1}(L - x_{jun})) - \Delta I_{B1} Zc_{OH_1} \sinh(\gamma_{OH1}(L - x_{jun}))$$
(8)

The formula given in (8) can be expressed as follows:
$$\Delta V_{SA1} \cosh(\gamma_{c1} x_{jun}) - \Delta I_{A1} Zc_{c1} \sinh(\gamma_{c1} x_{jun}) = \Delta V_{SB1} \cosh(\gamma_{OH1} L - \gamma_{OH1} x_{jun}) - \Delta I_{B1} Zc_{OH1} \sinh(\gamma_{OH1} L - \gamma_{OH1} x_{jun})$$
(9)

Using the following identities:
$$\sinh(u - v) = \sinh u \cosh v - \cosh u \sinh v$$
$$\cosh(u - v) = \cosh u \cosh v - \sinh u \sinh v,$$

The formula given in (9) can be expressed as follows:
$$\Delta V_{SA1} \cosh(\gamma_{c1} x_{jun}) - \Delta I_{A1} Zc_{c_1} \sinh(\gamma_{c1} x_{jun}) = \Delta V_{SB1} \cosh(\gamma_{OH1}L) \cosh(\gamma_{OH1} x_{jun}) - \Delta V_{SB1} \sinh(\gamma_{OH1}L) \sinh(\gamma_{OH1} x_{jun}) - \Delta I_{B1} Zc_{OH1} \sinh(\gamma_{OH1}L) \cosh(\gamma_{OH1} x_{jun}) + \Delta I_{B1} Zc_{OH1} \cosh(\gamma_{OH1}L) \sinh(\gamma_{OH1} x_{jun})$$
(10)

According to Taylor's expansion, the hyperbolic functions can be expanded as follows:

$$\sinh x = x + \frac{x^3}{3!} + \frac{x^5}{5!} + \cdots \ldots \ldots.$$
$$\cosh x = 1 + \frac{x^2}{2!} + \frac{x^4}{4!} + \cdots \ldots \ldots..$$

Then, the formula given in (10) can be rewritten as follows:
$$\Delta V_{SA1} \left(1 + \frac{\gamma_{c1}^2 x_{jun}^2}{2!} + \frac{\gamma_{c1}^4 x_{jun}^4}{4!} + \cdots \ldots \ldots \ldots \ldots \right) - \Delta I_{A1} Zc_{c_1} \left(\gamma_{c1} x_{jun} + \frac{\gamma_{c1}^3 x_{jun}^3}{3!} + \frac{\gamma_{c1}^5 x_{jun}^5}{5!} + \cdots \ldots \ldots. \right) = \Delta V_{SB1} \cosh\left((\gamma_{OH_1}L)\left(1 + \frac{\gamma_{OH_1}^2 x_{jun}^2}{2!} + \frac{\gamma_{OH_1}^4 x_{jun}^4}{4!} + \cdots \ldots \ldots \ldots \right) - \Delta V_{SB1} \sinh(\gamma_{OH_1}L) \left(\gamma_{OH_1} x_{jun} + \frac{\gamma_{OH_1}^3 x_{jun}^3}{3!} + \frac{\gamma_{OH_1}^5 x_{jun}^5}{5!} + \cdots \ldots \ldots \right) - \Delta I_{B1} Zc_{OH_1} \sinh(\gamma_{OH_1}L) \left(1 + \right.$$

$$\frac{\gamma_{OH_1}^2 x_{jun}^2}{2!} + \frac{\gamma_{OH_1}^4 x_{jun}^4}{4!} + \cdots \ldots \ldots \ldots \ldots \right) + \Delta I_{B1} Zc_{OH_1} \cosh(\gamma_{OH_1}L) \left(\gamma_{OH_1} x_{jun} + \frac{\gamma_{OH_1}^3 x_{jun}^3}{3!} + \frac{\gamma_{OH_1}^5 x_{jun}^5}{5!} + .. \right)$$
(11)

The formula in (11) can be rewritten as follows:
$$\Delta V_{SA1} - (\Delta I_{A1} Zc_{c_1} \gamma_{c1}) x_{jun} + \left(\frac{\Delta V_{SA1} \gamma_{c1}^2}{2!}\right) x_{jun}^2 - \left(\Delta I_{A1} \frac{Zc_{c1} \gamma_{c1}^3}{3!}\right) x_{jun}^3 + \left(\frac{\Delta V_{SA1} \gamma_{c1}^4}{4!}\right) x_{jun}^4 - \left(\Delta I_{A1} \frac{Zc_{c1} \gamma_{c1}^5}{5!}\right) x_{jun}^5 + \cdots = [\Delta V_{SB1} \cosh \gamma_{OH_1} L - \Delta I_{B1} Zc_{OH_1} \sinh \gamma_{OH_1}] + [\Delta I_{B1} Zc_{OH_1} \gamma_{OH_1} \cosh \gamma_{OH_1} L - \Delta V_{SB1} \gamma_{OH_1} \sinh \gamma_{OH_1} L] x_{jun} + [\frac{\Delta V_{SB1} \gamma_{OH_1}^2}{2!} \cosh \gamma_{OH_1} L - \Delta I_{B1} Zc_{OH_1} \frac{\gamma_{OH_1}^2}{2!} \sinh \gamma_2 L] x_{jun}^2 + \left[\Delta I_{B1} Zc_{OH_1} \cosh\cosh \gamma_{OH_1} L \frac{\gamma_{OH_1}^3}{3!} - \frac{\Delta V_{SB1} \gamma_{OH_1}^3}{3!} \sinh \gamma_{OH_1} L\right] x_{jun}^3 + [\frac{\Delta V_{SB1} \gamma_{OH_1}^4}{4!} \cosh \gamma_{OH_1} L - \Delta I_{B1} Zc_{OH_1} \frac{\gamma_2^4}{4!} \sinh \gamma_{OH_1} L] x_{jun}^4 + \left[\Delta I_{B1} Zc_{OH_1} \frac{\gamma_{OH_1}^5}{5!} \cosh \gamma_{OH_1} L - \frac{\Delta V_{SB1} \gamma_{OH_1}^5}{5!} \sinh \gamma_{OH_1} L\right] x_{jun}^5 \ldots..$$
(12)

For the 5th degree of expansion and by converting formula in (12) to a zero equation, it can be written in the following form:

$$a x_{jun}^5 + b x_{jun}^4 + c x_{jun}^3 + d x_{jun}^2 + e x_{jun} + g = 0$$
(13)

where these constants (a, b, c, d, e, and g) are as follows:

$$a = \left[\Delta I_{B1} Zc_{OH_1} \frac{\gamma_{OH_1}^5}{5!} \cosh \gamma_{OH_1} L - \frac{\Delta V_{SB1} \gamma_{OH_1}^5}{5!} \sinh \gamma_{OH_1} L + \Delta I_{A1} \frac{Zc_{c1} \gamma_{c1}^5}{5!}\right]$$
$$b = \left[\frac{\Delta V_{SB1} \gamma_{OH_1}^4}{4!} \cosh \gamma_{OH_1} L - \Delta I_{B1} Zc_{OH_1} \frac{\gamma_{OH_1}^4}{4!} \sinh \gamma_{OH_1} L - \frac{\Delta V_{SA1} \gamma_{c1}^4}{4!}\right]$$

$$c = \left[\Delta I_{B1} Zc_{OH_1} \frac{\gamma_{OH_1}^3}{3!} \cosh \gamma_{OH_1} L - \frac{\Delta V_{SB1} \gamma_{OH_1}^3}{3!} \sinh \gamma_{OH_1} L + \Delta I_{A1} \frac{Zc_{c1} \gamma_{c1}^3}{3!}\right]$$
$$d = [\frac{\Delta V_{SB1} \gamma_{OH_1}^2}{2!} \cosh \gamma_{OH_1} L - \Delta I_{B1} Zc_{OH_1} \frac{\gamma_{OH_1}^2}{2!} \sinh \gamma_{OH_1} L - \frac{\Delta V_{SA1} \gamma_{c1}^2}{2!}]$$
$$e = [\Delta I_{B1} Zc_{OH_1} \gamma_{OH_1} \cosh \gamma_{OH_1} L - \Delta V_{SB1} \gamma_{OH_1} \sinh \gamma_{OH_1} L + \Delta I_{A1} Zc_{c_1} \gamma_{c1}]$$
$$g = [\Delta V_{SB1} \cosh \gamma_{OH_1} L - \Delta I_{B1} Zc_{OH_1} \sinh \gamma_{OH_1} - \Delta V_{SA1}]$$
(14)

By using the initial guess for (x) as in [18], the roots of the formula given in (13) can be obtained numerically. The introduced identification method is also applicable to the

5

IEEE *Access*

combined transmission lines that consist of three segments, as in the following subsection.

A1. Combined line having three segments

The proposed concept is also applicable for combined transmission systems composed of three segments, such as line-cable-line combined networks. Fig. 3 shows a single-line diagram of a line-cable-line combined transmission system, such as the Taba-Aqaba Intertie transmission system. The identification of the faulted side is accomplished by applying the proposed concept twice at the two junction points (jun1 and jun2) between the adjacent sections, as illustrated in Figs. 4 and 5, and obtaining two distances (x_{jun1} and x_{jun2}), respectively. The two distances, x_{jun1} and x_{jun2}, are obtained by considering an artificial fault at either junction point, jun1 or jun2, irrespective of the actual fault point. Subsequently, the faulted side is determined by utilizing an introduced voting system (comparator) as follows:

If both values (x_{jun1} and x_{jun2}) indicate a fault on the cable section, then the faulted side is determined to be the cable section. This is illustrated in detail in Fig. 4 for a fault on the cable section. On the other hand, if both values (x_{jun1} and x_{jun2}) indicate a fault on an overhead section, then the faulted side is determined to be that overhead section. If one of the values indicates a fault on an overhead section and the other indicates a fault on the cable section, then the faulted side is determined to be the overhead section. The basic concept of this condition is illustrated in detail in Fig. 5 for a fault on the first overhead section. In other words, the first fault-side indicator (x_{jun1}) directly identifies faults occurring at the first overhead section, whereas the second indicator (x_{jun2}) directly identifies faults occurring at the second overhead section. However, faults occurring at the cable section are recognized by both indicators as cable faults. The conditions of the introduced comparator are summarized in Table 1. The calculation of two indicators x_{jun1} and x_{jun2} is as follows:

TABLE 1
THE PROPOSED COMPARATOR IDENTIFYING THE FAULTED SECTION

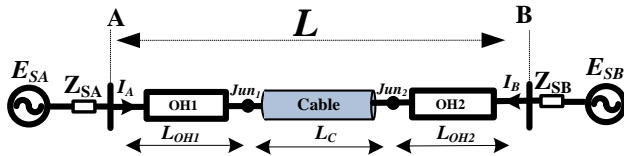| conditions		Decision
X_{jun1}	X_{jun2}	Fault at
$X_{jun1} < L_{OH1}$	$X_{jun2} < (L_{OH1}+L_c)$	OH1 side
$L_{OH1} < X_{jun1} < (L_{OH1}+L_c)$	$L_{OH1} < X_{jun2} < (L_{OH1}+L_c)$	Cable side
$X_{jun1} > L_{OH1}$	$X_{jun2} > (L_{OH1}+L_c)$	OH2 side
$X_{jun1} = L_{OH1}$	$X_{jun2} > X_{jun1}$	jun1
$X_{jun1} < X_{jun2}$	$X_{jun2} = (L_{OH1}+L_c)$	jun2

FIGURE 3. A cascaded line-cable-line combined transmission system.
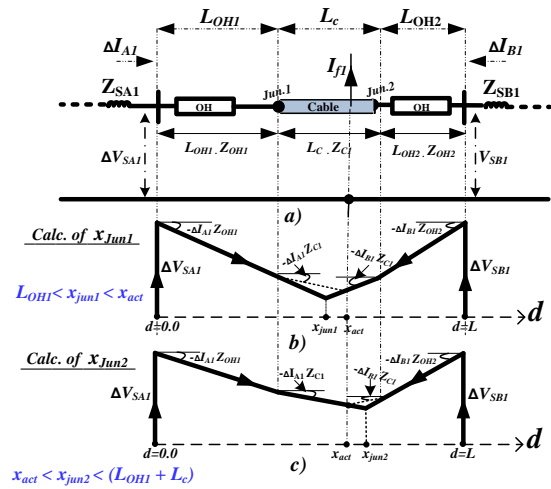

FIGURE 4. The pure positive-sequence circuit of a three-segment combined line under a fault on the cable side as in (a), and its voltage magnitude profile to obtain x_{jun1} as in (b) and x_{jun2} as in (c).
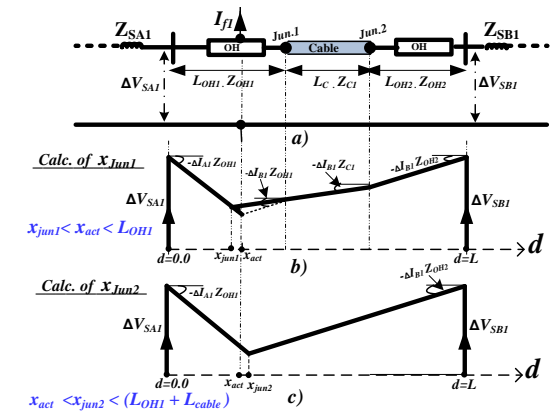

FIGURE 5. The pure positive-sequence circuit of a three-segment combined line under a fault on the first overhead section as in (a), and its voltage magnitude profile to obtain x_{jun1} as in (b) and x_{jun2} as in (c).

The calculation of x_{jun1} is performed by representing the combined transmission line as an overhead line combined with an underground cable, with terminals A and jun2. The change in positive-sequence voltage and current at jun2 is calculated based on the measured data at terminal B and the parameters of the overhead section 2 (OH2) connected to terminal B, as shown in (20).

$$\begin{vmatrix} \Delta V_{jun2_1} \\ \Delta I_{jun2_1} \end{vmatrix} = \begin{vmatrix} D_{OH2} & -B_{OH2} \\ -C_{OH2} & A_{OH2} \end{vmatrix} \cdot \begin{vmatrix} \Delta V_{SB1} \\ \Delta I_{B1} \end{vmatrix} \qquad (15)$$

where A_{OH2}, B_{OH2}, C_{OH2}, and D_{OH2} are the constants of the overhead line connected to busbar B considering the distributed line model representation.

The formula of x_{jun1} is derived by equating the two formulas that calculate the change in positive-sequence voltage at the first junction point, considering both sides A and jun2. These formulas utilize the distributed line model representation regardless of the actual fault point as shown in (16).

$$\Delta V_{SA1} \cosh(\gamma_{OH1} x_{jun1}) - \Delta I_{A1} Zc_{OH_1} \sinh(\gamma_{OH1} x_{jun1}) =$$
$$\Delta V_{jun2_1} \cosh\left(\gamma_{c1}(L_{OH1} + L_c - x_{jun1})\right) - \Delta I_{jun2_1}$$
$$Zc_{c1} \sinh\left(\gamma_{c1}(L_{OH1} + L_c - x_{jun1})\right) \qquad (16)$$

Therefore, x_{jun1} is obtained by solving a 5th degree equation, where the coefficients are presented in (17), similar to (14) with

6

changes in symbols for line terminals and the considered line length ($L_{OH1}+L_C$).

$$a = \left[\Delta I_{jun2_1} Zc_{c1} \frac{\gamma_{c1}^5}{5!} \cosh \gamma_{c1}(L_{OH1} + L_c) - \right.$$
$$\left. \frac{\Delta V_{jun2\_1} \cdot \gamma_{c1}^5}{5!} \sinh \gamma_{c1}(L_{OH1} + L_c) + \Delta I_{A1} \frac{Zc_{OH1} \cdot \gamma_{OH1}^5}{5!} \right]$$

$$b = \left[\Delta I_{jun2_1} Zc_{c1} \cosh h \, \gamma_{c1}(L_{OH1} + L_c) \frac{\gamma_{c1}^3}{3!} - \right.$$
$$\left. \frac{\Delta V_{jun2\_1} \cdot \gamma_{c1}^3}{3!} \sinh \gamma_{c1}(L_{OH1} + L_c) - \frac{\Delta V_{SA1} \cdot \gamma_{OH1}^4}{4!} \right]$$

$$c = \left[\frac{\Delta V_{jun2_1} \gamma_{c1}^3}{3!} \cosh \gamma_{c1}(L_{OH1} + L_c) - \right.$$
$$\left. \Delta I_{jun2_1} Zc_{c1} \frac{\gamma_{c1}^3}{3!} \sinh \gamma_{c1}(L_{OH1} + L_c) + \Delta I_{A1} \frac{Zc_{OH1} \gamma_{OH1}^3}{3!} \right]$$

$$d = \left[\frac{\Delta V_{jun2_1} \gamma_{c1}^2}{2!} \cosh \gamma_{c1}(L_{OH1} + L_c) - \right.$$
$$\left. \Delta I_{jun2_1} Zc_{c1} \frac{\gamma_{c1}^2}{2!} \sinh \gamma_{c1}(L_{OH1} + L_c) - \frac{\Delta V_{SA1} \gamma_{OH1}^2}{2!} \right]$$

$$e = \left[\Delta I_{jun2_1} Zc_{c1} \gamma_{c1} \cosh \gamma_{c1}(L_{OH1} + L_c) - \right.$$
$$\left. \Delta V_{jun2_1} \gamma_{c1} \sinh \gamma_{c1}(L_{OH1} + L_c) + \Delta I_{A1} Zc_{OH1} \gamma_{OH1} \right]$$

$$g = \left[\Delta V_{jun2_1} \cosh \gamma_{c1}(L_{OH1} + L_c) - \Delta I_{jun2_1} Z_{c1} \sinh \gamma_{c1} - \Delta V_{SA1} \right] \tag{17}$$

Similarly, under x_{jun2} calculation, the line can be represented as an underground cable combined with an overhead line where its terminals are jun1 and B. The change of positive-sequence voltage and current at jun1 is computed using the measured data at terminal A and the parameters of the overhead section connected to terminal A as shown in (18).

$$\begin{vmatrix} \Delta V_{jun1_1} \\ \Delta I_{jun1_1} \end{vmatrix} = \begin{vmatrix} D_{OH1} & -B_{OH1} \\ -C_{OH1} & A_{OH1} \end{vmatrix} \cdot \begin{vmatrix} \Delta V_{SA1} \\ \Delta I_{A1} \end{vmatrix} \tag{18}$$

where A_{OH1}, B_{OH1}, C_{OH1}, and D_{OH1} represent the constants of overhead line connected to busbar A, considering the distributed line model. The positive-sequence voltage at the second junction point, calculated from both sides jun1 and B, is equated using the distributed line model representation, regardless of the actual fault position, as shown in (19).

$$\Delta V_{jun1_1} \cosh(\gamma_{c1} x_{jun2}) - \Delta I_{jun1_1} Zc_{c1} \sinh(\gamma_{c1} x_{jun2}) =$$
$$\Delta V_{SB1} \cosh\left(\gamma_{OH1}(L_c + L_{OH2} - x_{jun2})\right) -$$
$$\Delta I_{B1} Zc_{OH1} \sinh\left(\gamma_{OH1}(L_c + L_{OH2} - x_{jun2})\right) \tag{19}$$

Also, x_{jun2} is obtained by solving a similar 5th degree equation where the coefficients are presented in (20), following a similar approach as in (14) but with changes in the symbols of line terminals and the considered line length ($L_C + L_{OH2}$). Subsequently, the length of the overhead section 1 (L_{OH1}) is added to establish the reference of the obtained distance as Busbar A.

$$a = \left[\Delta I_{B1} Zc_{OH1} \frac{\gamma_{OH1}^5}{5!} \cosh \gamma_{OH1}(L_c + L_{OH2}) - \right.$$
$$\frac{\Delta V_{SB1} \gamma_{OH1}^5}{5!} \sinh \gamma_{OH1}(L_c + L_{OH2}) + \Delta I_{jun1_1} \frac{Zc_{c1} \gamma_{c1}^5}{5!} \Big]$$

$$b = \left[[\Delta I_{B1} Zc_{OH1} \cosh h \, \gamma_{OH1}(L_c + L_{OH2}) \frac{\gamma_{OH1}^3}{3!} - \right.$$
$$\frac{\Delta V_{SB1} \gamma_{OH1}^3}{3!} \sinh \gamma_{OH1}(L_c + L_{OH2}) - \frac{\Delta V_{jun1_1} \gamma_{c1}^4}{4!} \Big]$$

$$c = \left[\Delta I_{B1} Zc_{OH1} \frac{\gamma_{OH1}^3}{3!} \cosh \gamma_{OH1}(L_c + L_{OH2}) - \right.$$
$$\frac{\Delta V_{SB1} \gamma_{OH1}^3}{3!} \sinh \gamma_{OH1}(L_c + L_{OH2}) + \Delta I_{jun1_1} \frac{Zc_{c1} \gamma_{c1}^3}{3!} \Big]$$

$$d = \left[\frac{\Delta V_{SB1} \gamma_{OH1}^2}{2!} \cosh \gamma_{OH1}(L_c + L_{OH2}) - \right.$$
$$\Delta I_{B1} Zc_{OH1} \frac{\gamma_{OH1}^2}{2!} \sinh \gamma_{OH1}(L_c + L_{OH2}) - \frac{\Delta V_{jun1_1} \gamma_{c1}^2}{2!} \Big]$$

$$e = \left[\Delta I_{B1} Zc_{OH1} \gamma_{OH1} \cosh \gamma_{OH1}(L_c + L_{OH2}) - \right.$$
$$\Delta V_{SB1} \gamma_{OH1} \sinh \gamma_{OH1}(L_c + L_{OH2}) + \Delta I_{jun1_1} Zc_{c1} \gamma_{c1} \Big]$$

$$g = \left[\Delta V_{SB1} \cosh \gamma_{OH1}(L_c + L_{OH2}) \, \Delta I_{B1} Zc_{OH1} \sinh \gamma_{OH1}(L_c + L_{OH2}) - \Delta V_{jun1_1} \right] \tag{20}$$

Finally, the faulted section is precisely identified by analyzing the two values of x_{jun1} and x_{jun2}, as shown in Table 1. Then, the actual fault distance is directly obtained as described in the following subsection.

B. Fault-locator algorithm

After gathering the measured data from the ends of the combined line, the symmetrical components of measured three-phase voltages and currents are computed. The identification of the faulted section, as presented in the above subsection, is then accomplished. Additionally, the positive-sequence data at the terminals of the obtained faulted section are prepared, as mentioned above. The fault location estimation is carried out based on the obtained faulted section. For example, let's consider a fault on the cable section of the combined line, which has three segments as illustrated in Fig. 4. The fault location is determined as follows: The two values of x_{jun1} and x_{jun2} indicate a fault on the cable section, and therefore the obtained faulted side is the cable section. Furthermore, the positive sequence voltage and current at the two junction points jun1 and jun2 (V_{jun11}, I_{jun11}, V_{jun21}, I_{jun21}) are estimated as mentioned above. Then, the fault location is estimated by equating the positive sequence voltage of fault point as a function of the estimated data at the two junction points as;

$$V_{f1_1} = V_{jun1_1} \cosh(\gamma_{c1} x) - I_{jun1_1} Zc_{c1} \sinh(\gamma_{c1} x) =$$
$$V_{jun2_1} \cosh(\gamma_{c1}(L_c - x)) - I_{jun2_1} Zc_{c1} \sinh(\gamma_{c1}(L_c - x)) \tag{21}$$

Hence, the fault distance (x) is estimated as in (22) and then adding the L_{OH1} length to be referred to the Busbar A.

$$x =$$
$$\frac{1}{\gamma_{c1}} \cdot \tanh^{-1} \left(\frac{V_{jun2_1} \cosh(\gamma_{c1} L_c) - I_{jun2_1} Zc_{c1} \sinh(\gamma_{c1} L_c) - V_{jun1_1}}{V_{jun2_1} \sinh(\gamma_{c1} L_c) - I_{jun2_1} Zc_{c1} \cosh(\gamma_{c1} L_c) - I_{jun1_1} Zc_{c1}} \right) \tag{22}$$

7

Similarly, the fault location is also obtained under faults on the overhead sections. For example, for faults on the overhead section 2, a similar formula to that shown in (22) is utilized with some changes. These changes are replacing the cable parameters with these faulted overhead section parameters as well as using the data at Junction 2 and Busbar B instead of that at Junction 1 and Junction 2, respectively. To be the obtained distance referred to the Busbar A, the lengths of both L_{OH1} and L_c should be added.

Finally, the presented scheme can be implemented in the intertie combined transmission line by first identifying the faulted section and then locating the fault point. In combined transmission systems with two segments, the faulted section is identified by analyzing the value of the fault-side indicator (x_{jun}) obtained from (14), as illustrated in Fig. 6. For combined transmission systems with three segments, the faulted section is identified by analyzing the values of the two computed distances, x_{jun1} and x_{jun2}, as shown in both Table 1 and Fig. 7. These two computed distances (x_{jun1} and x_{jun2}) are obtained by solving a 5th-degree equation, where their coefficients are presented in (17) and (20), respectively.

After identifying the faulted section, the positive-sequence voltages and currents at the two ends of the faulted section are calculated. The fault location is then determined using these calculated values and the parameters of the faulted section. For example, if the fault occurs on the cable section of the three-segment combined line, the fault distance is obtained as described in (22).

III. Simulation of Actual Combined Transmission Line

To accomplish the aimed study, an actual nonhomogeneous transmission line connecting the Egyptian and Jordanian networks is studied. Fig. 8 illustrates the selected power system network from 500 kV Eyoun-Mousa station in Egypt to 400 kV Aqaba station in Jordan including the following parts:
- 500 kV, 244 km length, overhead transmission line starting from Eyoun-Mousa station to 500 kV Taba substation.
- 750 MVA, 500/400/22 kV three-phase autotransformer (consisting of three-single phase ones).
- 400 kV, 20 km overhead transmission line connecting between 500 kV Taba substation and Egyptian submarine cable side.
- 400 kV, 13.6 km three single core submarine cable linking Egyptian and Jordanian networks.
- 400 kV, 10 km overhead line linking the submarine cable with 400 kV Aqaba station.
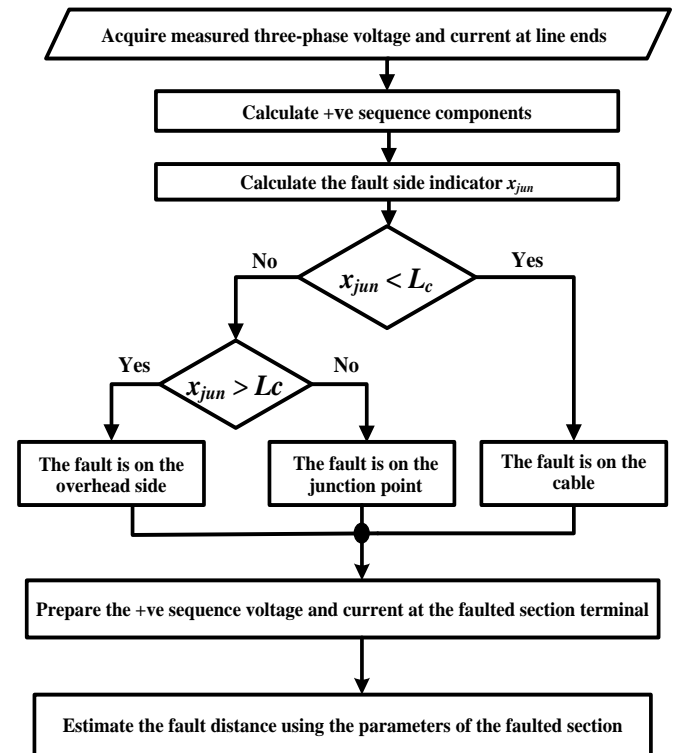

FIGURE 6. The presented algorithm flowchart for a two segments transmission line.

As shown from these elements, Taba-Aqaba inter-tie transmission system represents an actual system for evaluating the associated problems with the fault-locator techniques for composite lines. The appendix includes the parameter data for simulated overhead sections and simulated underground section. ATP/EMTP package is used for simulating the considered actual system.

IV. The Proposed Scheme Assessment

Different fault cases were prepared in the ATP package using 32 samples per cycle at various points, covering the entire range of the line, including faults close to tie points between the different segments. The fundamental frequency components of the three-phase voltage and current phasors are calculated using the cosine filter. The cosine filter cancels exponentially decaying DC offsets, cancels all harmonics, approximates desirable bandpass filtering, and has a perfect transient response [19]. The cosine filter outperforms the Fourier filter in the presence of DC offsets. Subsequently, the presented faulted section identification method and the fault-locator technique are carried out sequentially. Finally, the error is computed as a percentage of the length of the faulted segment.

The studied cases can be categorized as follows:
Case 1: Different fault types, fault distances, and fault resistance effects.
Case 2: Effect of nonlinear fault resistance (arcing fault).
Case 3: Effect of changing the source impedance.
Case 4: Effect of changing the fault impedance.

8

A. *Simulation results: Case 1*

The presented faulted-side identification method and the fault locator were tested for both line-to-ground, line-to-line, line-to-line-to-ground, and three-phase faults, as shown in Tables 2, 3, 4, and 5, respectively. The tests considered faults close to the junction point.

From the results, one can observe that, during faults on the cable section, the values of two obtained indicators (x_{jun1} and x_{jun2}) fall within the range of 20 to 33.6 km for all fault types. Thus, the output of the presented comparator indicates a fault in the cable section, as listed in Tables 2, 3, 4, and 5. On the other hand, during faults on the first overhead section OH1, the value of x_{jun1} is less than 20 km, and xjun2 is also less than 33.6 km. This output of the comparator indicates a fault in the OH1 section. Similarly, for faults on the second overhead section OH2, the value of x_{jun1} is greater than 20 km, and x_{jun2} is greater than 33.6 km. The comparator's output indicates a fault in the OH2 section. The results prove that the presented faulted side identification method is successful even under faults close to the junction points (jun1 and jun2), as shown in the shaded rows in Table 6. Therefore, the fault location algorithm accurately pinpoints the fault location after identifying the faulted section,

where the maximum error is 0.837% of the faulted segment only, as shown in the right-hand side column in Table 6. Finally, the results demonstrate the efficacy of the proposed algorithms. Although the proposed scheme is accurate under faults close to the junction points connecting the cable section to the overhead lines' sections (demonstrated both theoretically in the paper, Section II, and through the obtained results), if the scheme's output indicates a fault within the 20 m threshold around a junction point, it signifies that the fault is around the corresponding junction point.

TABLE 3
THE PROPOSED SCHEME PERFORMANCE UNDER L-TO-L FAULTS ASSOCIATED WITH 20 Ω FAULT RESISTANCE.

Faulted side	Fault at (km)	x_{jun1} (km)	x_{jun2} (km)	Obtained faulted side	Estimated Distance (km)	Error (%)
OH1	10	8.35	13.05	OH1 Side	10.0236	0.118
	15	13.902	18.423		15.0173	0.0865
	19.95	19.90	24.17		19.928	0.11
	19.98	19.96	24.35		19.944	0.18
Cable	20.03	20.026	24.374	Cable Side	20.073	0.316
	20.06	20.049	24.391		20.106	0.338
	25	23.546	30.869		25.035	0.2574
	30	24.975	32.366		30.046	0.3382
	33.4	26.273	33.558		33.372	0.206
	33.55	26.342	33.572		33.511	0.2868
OH2	33.65	27.836	33.878	OH2 Side	33.707	0.57
	33.7	28.053	33.995		33.758	0.58
	35	31.189	36.642		35.054	0.54
	40	37.586	41.957		40.0619	0.619

TABLE 4
THE PROPOSED SCHEME PERFORMANCE UNDER L-TO-L-TO-G FAULTS ASSOCIATED WITH 30 Ω FAULT RESISTANCE.

Faulted side	Fault at (km)	x_{jun1} (km)	x_{jun2} (km)	Obtained faulted side	Estimated Distance (km)	Error (%)
OH1	10	8.104	13.243	OH1 Side	10.031	0.155
	15	13.617	18.876		15.027	0.135
	19.95	19.93	24.937		19.924	0.13
	19.98	19.958	25.114		19.936	0.22
Cable	20.03	20.025	25.283	Cable Side	20.052	0.162
	20.06	20.053	25.342		20.104	0.3235
	25	22.944	31.576		25.018	0.1324
	30	23.416	31.786		30.0671	0.4934
	33.4	24.568	33.582		33.386	0.103
	33.55	25.105	33.591		33.539	0.081
OH2	33.65	27.562	33.892	OH2 Side	33.692	0.42
	33.7	27.249	33.998		33.766	0.66
	35	30.738	36.913		35.032	0.32
	40	37.264	42.043		40.0617	0.617

TABLE 2
THE PROPOSED SCHEME PERFORMANCE UNDER L-TO-G FAULTS ASSOCIATED WITH 10 Ω FAULT RESISTANCE.

Fault side	Fault at (km)	x_{jun1} (km)	x_{jun2} (km)	Obtained faulted side	Estimated Distance (km)	Error (%)
OH1	0.4	0.251	0.48	OH1 Side	0.419	0.095
	8	5.834	9.97		8.0104	0.052
	12	10.542	14.80		12.005	0.025
	16	15.187	19.15		15.974	0.13
	19.6	19.415	22.95		19.567	0.165
	19.9	19.833	23.14		19.876	0.12
	19.95	19.926	23.23		19.913	0.185
	19.98	19.978	23.42		19.948	0.16
Cable	20.03	20.027	23.764	Cable Side	20.057	0.1985
	20.06	20.053	24.152		20.075	0.11
	20.09	20.074	24.423		20.16	0.5147
	20.1	20.075	25.226		20.14	0.2941
	25	23.603	30.269		25.0821	0.604
	28	24.847	31.732		28.004	0.03
	30	25.324	31.681		29.989	0.081
	32	26.254	33.084		31.988	0.088
	33	26.969	33.325		32.981	0.1397
	33.2	27.805	33.479		33.195	0.037
	33.4	27.921	33.544		33.384	0.1176
	33.55	28.042	33.563		33.533	0.125
OH2	33.65	28.153	33.846	OH2 Side	33.698	0.48
	33.7	28.169	33.925		33.786	0.86
	33.75	28.438	34.072		33.792	0.42
	33.8	28.617	34.113		33.885	0.85
	35	31.283	36.335		35.0174	0.174
	37	33.694	38.524		37.046	0.46
	40	37.732	41.717		40.078	0.78
	42	40.351	42.964		42.0837	0.837

9

TABLE 5
THE PROPOSED SCHEME PERFORMANCE UNDER THREE PHASE FAULTS
ASSOCIATED WITH 50 Ω FAULT RESISTANCE.

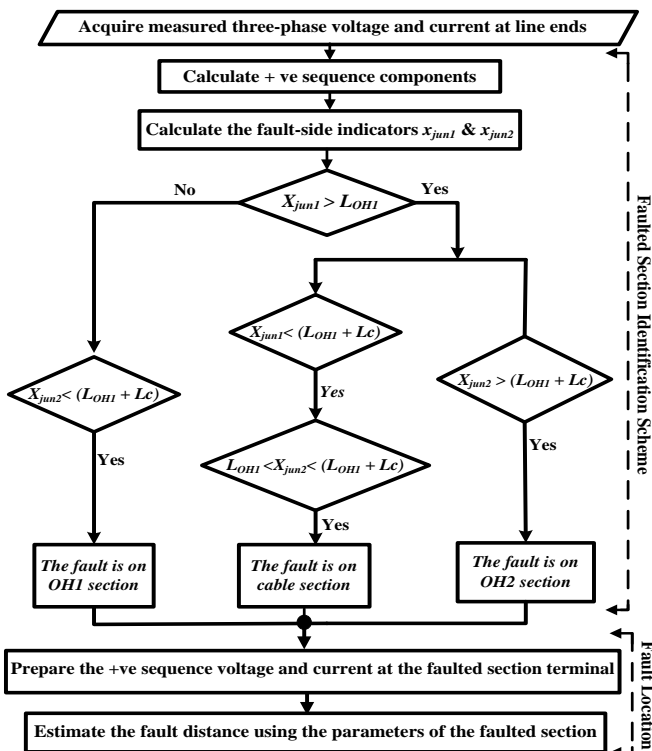| Faulted side	Fault at (km)	x_{jun1} (km)	x_{jun2} (km)	Obtained faulted side	Estimated Distance (km)	Error (%)
OH1	10	7.688	13.326	OH1 Side	10.029	0.145
	15	13.232	19.132		15.031	0.155
	19.95	19.896	25.095		19.9301	0.0995
	19.98	19.949	25.213		19.942	0.19
Cable	20.03	20.020	25.408	Cable Side	20.063	0.243
	20.06	20.048	25.554		20.152	0.676
	25	22.551	31.792		25.031	0.228
	30	23.253	32.241		30.0596	0.438
	33.4	24.432	33.589		33.357	0.316
	33.55	24.945	33.592		33.541	0.066
OH2	33.65	25.650	33.921	OH2 Side	33.667	0.17
	33.7	25.919	34.105		33.803	1.03
	35	30.447	37.168		35.044	0.44
	40	37.153	42.171		40.072	0.72

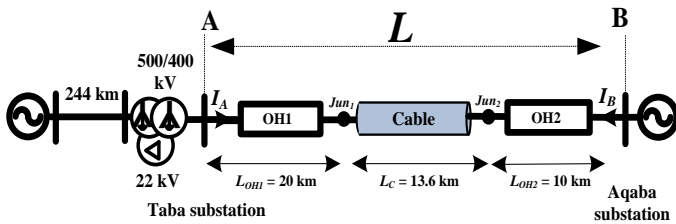FIGURE 7. The introduced algorithm flowchart for Taba-Aqaba transmission Line.

FIGURE 8. A single line diagram of Taba-Aqaba inter-tie system configuration.

B. Simulation results: Case 2

The previous results are with fixed fault resistance whatever its value. In this case, the performance of the

presented protection scheme was investigated during an arcing fault, in which the fault resistance is nonlinear based on the arcing model presented in [20]. The arcing model is depicted in Fig. 9. The model is based on energy balance in the arc [20] and is characterized by the following differential equation:

$$\frac{dg}{dt} = \frac{1}{\tau}(G - g) \tag{23}$$

where τ is the arc time constant. G and g are the stationary and instantaneous arc conductance, respectively.

The stationary arc conductance is defined as:

$$G = \frac{|i_{arc}|}{(U_O + R \cdot |i_{arc}|)l_{arc}} \tag{24}$$

where i_{arc} is instantaneous arc current. U_O and R are the constant voltage and the resistive component parameter per arc length, respectively. The values of parameters U_O, R, and τ are 13.5 V/cm, 1 mΩ/cm, and 0.8 ms, respectively.
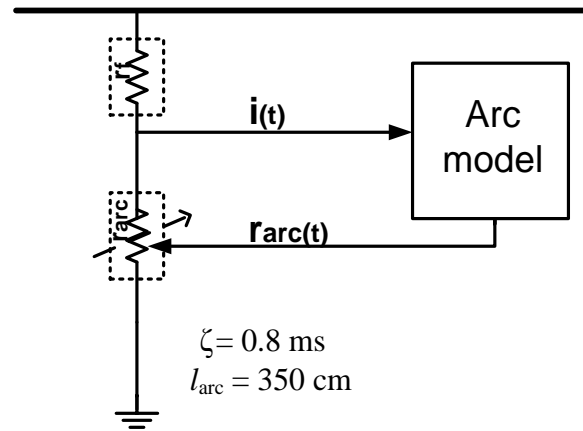

FIGURE 9. Arc model structure

One example of an arcing fault occurring at 23.6 km from terminal A is carried out to test the proposed algorithm. Fig. 10 illustrates the simulated arc characteristic (arc voltage, arc resistance, and I-V characteristic). Fig. 11 shows the measured three-phase current and voltage under the simulated arcing fault and the response of the cosine filter. Fig. 12 shows the response of the presented algorithm under this arcing fault. Figs. 12.a and 12.b show the output of the first and second fault-side indicators (x_{jun1} and x_{jun2}) where the two values indicate that the fault is on the cable side. Then, the presented algorithm identifies the faulted section. Fig. 12.c shows the estimated fault distance and confirms the reliability of the presented algorithm for the Taba-Aqaba Intertie transmission system under arcing faults (nonlinear faults).
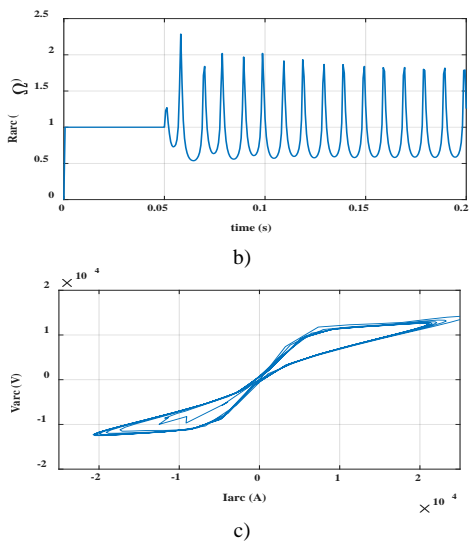

a)

10

b)

c)
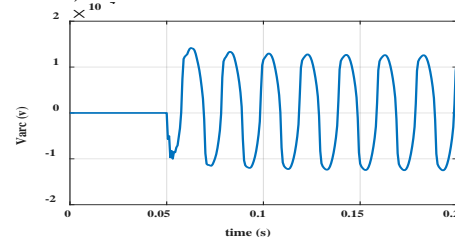
FIGURE 10. The simulated arc characteristic illustrating the (a) arc voltage, (b) arc resistance, and (c) I-V characteristic.

C. Simulation results: Case 3

The presented scheme was also investigated by varying the source impedance. In this test case, +/-10% range is utilized in varying the source impedance with a line-to-ground fault at 25 km distance. Table 6 depicts the results obtained, which validate the efficacy of the presented scheme.
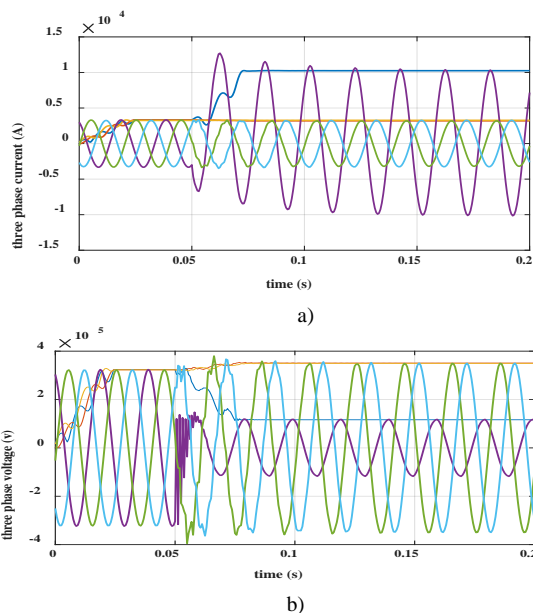

a)

b)

FIGURE 11. The measured three-phase current and voltage under an arcing fault at 23.6 km distance from terminal A and the response of the cosine filter.

TABLE 6

THE PROPOSED SCHEME PERFORMANCE UNDER VARIATION OF THE SOURCE IMPEDANCE.

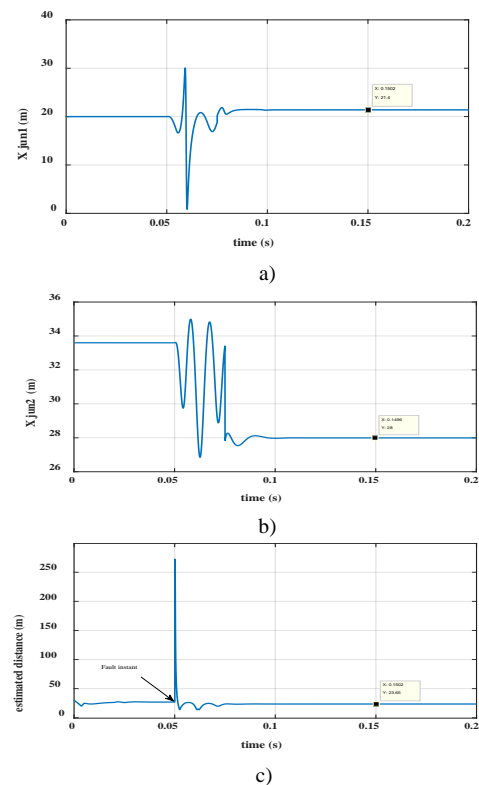| Impedance Z1sA (Ω)	Impedance Z1sB (Ω)	x_{jun1} (km)	x_{jun2} (km)	Estimated Distance (km)
0.724+ j8.25	1.44+j16.5	23.603	30.269	25.0821
0.796+j9.075	1.584+j18.15	23.712	30.294	25.0865
0.6516+j7.425	1.296+j14.85	23.478	30.133	25.0734

a)

b)

c)

FIGURE 12. The response of the presented algorithm under non-linear fault resistance at 23.6 km fault distance where (a) Xjun1, (b) Xjun2, and (c) estimated distance.

D. Simulation results: Case 4

Testing of the proposed scheme was conducted by varying the fault impedance, specifically considering high impedance faults. To achieve this, we introduced different line-to-ground faults within the cable section located at a 30 km distance from terminal A, with fault impedances ranging from 0.1 Ω to 1 kΩ. The results of these tests, as illustrated in Fig. 13, which shows the outputs of the scheme versus the selected fault circumstances, confirmed that the proposed scheme remains effective and independent of the fault impedance variations.
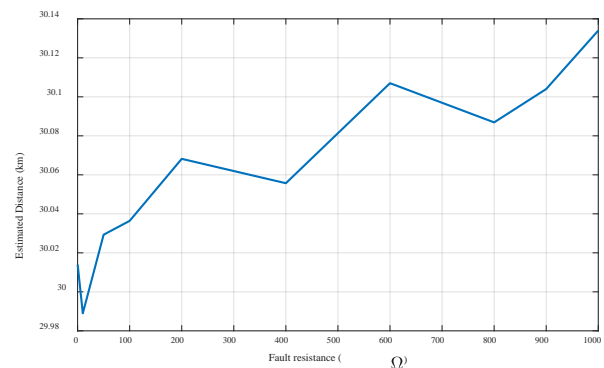

FIGURE 13. The response of the presented algorithm under line-to-ground faults with varying the fault impedance.

11

V. Conclusions

A new fault location scheme for an actual overhead line-submarine cable-overhead transmission system (Taba-Aqaba Inter–Tie transmission system) is introduced. The proposed algorithm depends on identifying the faulted section by introducing new fault-side indicators. The fault-side indicators (x_{jun1} and x_{jun2}) are the calculated distances under considering an artificial fault at either the first or second junction point regardless of the actual fault point. Then, a new voting system is used to obtain the faulted zone. In other words, the first fault-side indicator (x_{jun1}) directly refers to faults occurring at the first overhead section, whereas the second indicator (x_{jun2}) directly refers to faults occurring at the second overhead section. However, the faults occurring at the cable section must be seen by the two indicators as cable faults. The introduced identification method depends on the rate of change of the voltage along the nonhomogeneous line in the pure positive-sequence circuit by exploiting the inequality of positive-sequence impedances of both power cable and overhead line. The proposed scheme is investigated under different simulation cases using ATP-EMTP.

The results confirmed the high efficacy of the proposed faulted section determination. The proposed scheme is unaffected by variations in source impedance, fault types, and zero-sequence circuit parameters making it applicable for submarine cables. Additionally, the proposed algorithm is reliable under nonlinear faults. Consequently, the fault location can be determined straightforwardly by equating the formulae of positive-sequence voltage at the fault point, derived as a function of the data at the obtained faulted section terminals. An essential future prospect of this paper involves enhancing the presented scheme's applicability under unsynchronized data considering dynamic loading effect.

VI. REFERENCES

[1] M. Bawart, M. Marzinotto, and G. Mazzanti, "A deeper insight into fault location on long submarine power cables," *CIGRE*, pp. 355–360, Dec. 2014.

[2] A. D. Zahran, N. I. Elkalashy, M. A. Elsadd, T. A. Kawady and A. I. Taalab, "Improved ground distance protection for cascaded overhead-submarine cable transmission system," *2017 Nineteenth International Middle East Power Systems Conference (MEPCON)*, Cairo, 2017, pp. 778-758.

[3] M. Gilany, D. K. Ibrahim, and E. S. T. Eldin, "Traveling-wave-based fault-location scheme for multiend-aged underground cable system," *IEEE Trans. Power Deliv.*, 2007, vol. 22, no.1, pp. 82-89.

[4] A. Swetapadma and A. Yadav, "A novel decision tree regression based fault distance estimation scheme for transmission lines," *IEEE Trans. Power Del.*, vol. PP, no. 99, Aug. 2016.

[5] M. A. Elsadd and A. Y. Abdelaziz, "Unsynchronized fault-location technique for two- and three-terminal transmission lines," *Elec. Power Syst. Research*, vol. 158, pp. 228-239, May 2018.

[6] H. Livani and C.Y. Evrenosoglu, "A machine learning and wavelet-based fault location method for hybrid transmission lines, *IEEE Trans. Smart Grid,* vol. 5, no. 1, pp. 51–59, 2014.

[7] J. Sadeh and H. Afradi, "A new and accurate fault location algorithm for combined transmission lines using Adaptive Network-Based Fuzzy Inference System, *Electr. Power Syst. Res.,* vol. 79, pp. 1538–1545, 2009.

[8] Bikash Patel, "A new FDOST entropy based intelligent digital relaying for detection, classification and localization of faults on the hybrid transmission line", *Elec. Power Syst. Research*, vol. 157, pp. 39–47, 2018.

[9] M. Gilany, E. T. El Din, M. M. Abdel Aziz, and D. k. Ibrahim, "Travelling wave-based fault location scheme for aged underground cable combined with overhead line," *International Journal of Emerging Electric Power Systems*, vol. 2, no. 2, 2005.

[10] A. B. M. S. Azam, W. H. Schmidt, K. Elford, and C. Knudstrup, "Dynamic loading effect on fault current and arc flash for a coordinated substation," *IEEE Access*, vol. 9, pp. 94309-94317, 2021.

[11] M. Gilany, E. T. El Din, M. M. Abdel Aziz, and D. k. Ibrahim, "An accurate scheme for fault location in combined transmission line with underground power cable," *Proc. IEEE Power Eng. Soc. Gen. Meet.*, San Francisco, vol. 3, pp. 2521–2527, 2005.

[12] E. T. El Din, M. M. Abdel Aziz, and D. k. Ibrahim, M. Gilany, "Fault location scheme for combined overhead line with underground power cable," *Elec. Power Syst. Research*, vol. 76, no. 11, pp. 928–935, July 2006.

[13] C. W. Liu, T. C. Lin, C. S. Yu, and J. Z. Yang, "A fault location technique for two-terminal multisession compound transmission lines using synchronized phasor measurements," *IEEE Trans. Smart Grid*, vol. 3, no. 1, pp. 113-121, Mar. 2012.

[14] T. C. Lin, P. Y. Lin, and C. W. Liu, "An algorithm for locating faults in three-terminal multisection nonhomogeneous transmission lines using synchrophasor measurements," *IEEE Trans. Smart Grid.*, vol. 5, no. 1, pp. 38-50, Jan. 2014.

[15] S. M. Hashemian, S. N. Hashemian, and M. Gholipour, "Unsynchronized parameter free fault location scheme for hybrid transmission line", *Elec. Power Syst. Research,* vol. 192, 2021.

[16] H. Shu, X. Liu, and X. Tian, "Single-ended fault location for hybrid feeders based on characteristic distribution of traveling wave along a line", *IEEE Transactions on Power Delivery*, vol. 36, no. 1, pp. 339 – 350, 2021.

[17] D. Rezaei, M. Gholipour, and F. Parvaresh, "A single-ended traveling-wave-based fault location for a hybrid transmission line using detected arrival times and TW′s polarity", *Elec. Power Syst. Research* vol. 210, 2022.

[18] M. Elsadd, N. Elkalashy, T. Kawady, A. Taalab, and M. Lehtonen, "Incorporating earth fault location in management control scheme for distribution networks", *IET Generation, Transmission & Distribution*, vol.10, 2016.

[19] E. O. Schweitzer and D. Hou, "Filtering for protective relays. In IEEE WESCANEX 93 Communications", *Computers and Power in the Modern Environment-Conference Proceedings*, pp. 15-23, May 1993.

[20] M. Kizilcay and T. Pniok, "Digital simulation of fault arcs in power systems", *European Transactions on Electrical Power*, vol. 1, no. 1, pp. 55-60, 1991.

VII. Appendix

The Configuration of Taba-Aqaba Cascaded Transmission Line is as follows:

A. Simulated Overhead configuration

The configuration of the simulated overhead is depicted in Fig. 14. Additionally, the dimensions of the utilized towers and the parameters of the overhead line per unit length in km are shown in Tables 7 and 8, respectively.
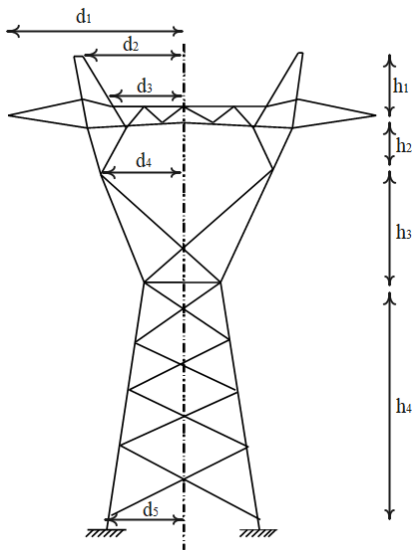
FIGURE 14. The utilized tower configuration for the overhead Transmission line.

Table 7:   Dimensions of the utilized towers (in meters)

d_5	d_4	d_3	d_2	d1	h4	h3	h2	h1
4.22	6.1	7.0	10.15	16.4	3.25	5.86	10.79	16.59

Table 8:   Parameters of overhead line

Positive-sequence impedance per km	$0.3853 \ \Omega \ \angle 84.351^{o}$
Zero-sequence impedance per km	$0.9062 \ \Omega \ \angle 84.257^{o}$
Positive-sequence shunt admittance per km	$3.4226e\text{-}06 \ \mho \angle 94.758^{o}$
Zero-sequence shunt admittance per km	$1.7584e\text{-}06 \ \mho \angle \ 94.82^{o}$

B.   Simulated single core cable configuration

The configuration of the simulated cable is depicted in Fig. 15. Additionally, the parameters of the cable section per unit length in km are shown in Table 9.

Table 9:   Parameters of cable

Positive-sequence impedance per km	$0.0951 \ \Omega \ \angle 58.757^{o}$
Zero-sequence impedance per km	$0.0789 \ \Omega \ \angle 49.268^{o}$
Positive-sequence shunt admittance per km	$6.8044e\text{-}05 \ \mho \angle 90^{o}$
Zero-sequence shunt admittance per km	$6.1044e\text{-}05 \ \mho \angle 90^{o}$

Weight in air: 57.7 kg/m
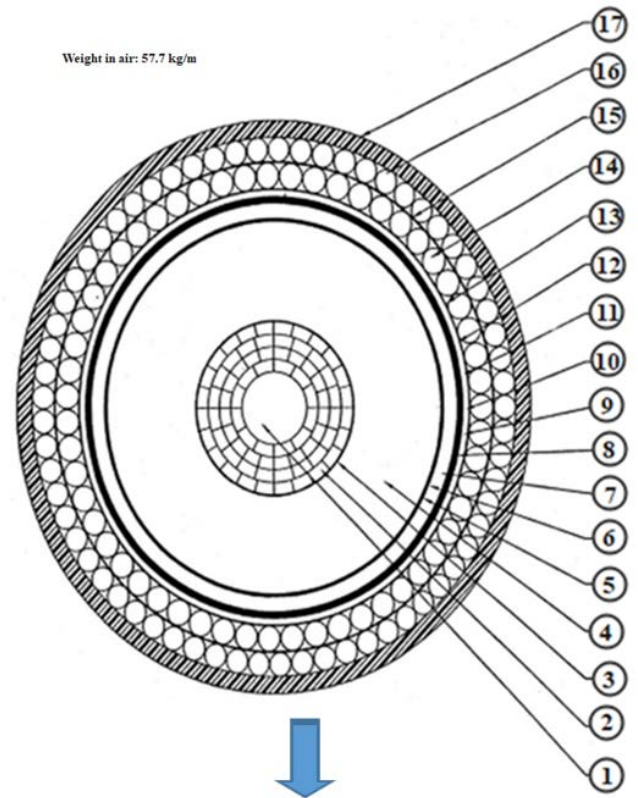
Position	Quantity	Description	Thickness (m)
1		Oil Duct	
2		Conductor Copper	
3	2	Carbon Black Paper Tapes	
4		Insulation, Impregnated Paper Tapes	22.9
5		Carbon Black Paper and Metalized Paper Tapes	
6	2	Copper Woven Fabric Tape	
7		Lead Sheath, Alloy F3	3.5
8	1	Copper Woven Fabric Tape	0.25
9	2	Transversal Reinforced, Stainless-Steel Tapes	0.2
10	1	Copper Woven Fabric Tape	0.25
11	2	Return Conductor Tinned Copper Tapes	0.34
12	2	Chloroprene Jacket, Semiconductive	1.5
13	1	Semiconducting Nylon Tapes	0.2
14	54	Armour, Galvanized Steel Wires	d=6.0
15	1	Semiconducting Nylon Tapes	0.2
16	65	Armour, Galvanized Steel Wires	d=5.6
17		Covering, Polypropylene Yarn and Asphalt	

FIGURE 15. Cross-sectional area of the used single-core cable and its relevant parameters.

13

MAHMOUD A. Elsadd was born in Menoufia, Egypt, on October 1, 1985. He received the B.Sc., M.Sc., and Ph.D. degrees in Electrical Engineering from Menoufia University, Shebin El-Kom, Egypt, in 2007, 2012, and 2016, respectively.

He held the position of teaching assistant in 2007, then an assistant teacher in 2012, then an assistant professor in 2016 at the Department of Electrical Engineering, Faculty of Engineering, Menoufia University, Shebin El-kom, Egypt. In 2021, he became an associate professor at the Department of Electrical Engineering, Faculty of Engineering, Menoufia University, Shebin El-kom, Egypt. He is now an associate professor at the Department of Electrical Engineering, Faculty of Engineering, Damanhour University, Egypt. His research interests include fault management in smart grids using various control schemes, security and privacy protection within smart grids, HVDC link protection, optimization techniques for power system operation, control system design, applications of Artificial Intelligence, solar and wind energy systems, and power system protection.

Ahmed R. Adly received the B.Sc., M.Sc. and PhD degrees in electrical engineering from Menoufia University, Cairo University, and Ain Sham University Egypt, in 2007, 2012, and 2017 respectively. He is currently Assoc. Prof. at the second research reactor—Atomic Energy Authority, Cairo, Egypt. His research interests are in the operation of smart grid, nuclear power plant, power quality, power system protection, transmission lines, line protection, and relaying scheme.
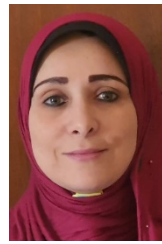
Hala A. Omar was born in Menoufia, Egypt, on October 1, 1978. She received a B.Sc. (Hons.) degree in electrical engineering from Menofia University, Shebin El-Kom, Egypt, in 2000. She received M.Sc. and Ph.D. in engineering mathematics from Minoufia University, Shebin Elkom, Egypt, in 2009 and 2013, respectively. Currently, she has been an Assistant Professor at Minoufia University since 2013. Her interests are in Numerical computations, Differential equations, Artificial Intelligence applications, and numerical stability analysis.

Ahmed Faheem Zobaa received his BSc (Hons), MSc, and PhD degrees in Electrical Power & Machines from Cairo University, Egypt, in 1992, 1997, and 2002, respectively. He received his Postgraduate Certificate in Academic Practice from the University of Exeter, the UK, in 2010, and his Doctoral of Science from Brunel University London, the UK, in 2017. He was an instructor from 1992–1997, a Teaching Assistant from 1997–2002, and an Assistant Professor from 2002–2007 at Cairo University, Egypt. From 2007 to 2010, he was a Senior Lecturer in renewable energy at the University of Exeter, UK. From 2010 to 2019, he was a Senior Lecturer in power systems at Brunel University London, UK. He is currently a Reader in electrical and power engineering and a Member of the Brunel Interdisciplinary Power Systems Research Centre at Brunel University London, UK. His main areas of expertise include power quality, (marine) renewable energy, smart grids, energy efficiency, and lighting applications.

Dr Zobaa is Executive Editor-in-Chief for *Smart Grids and Sustainable Energy Journal*. He is also an Editorial Board member, Editor, Associate Editor, and Editorial Advisory Board member for many international journals. He is a registered Chartered Engineer, Chartered Energy Engineer, European Engineer, and International Professional Engineer. He is also a registered member of the Engineering Council, UK; the Egypt Syndicate of Engineers; and the Egyptian Society of Engineers. He is a Senior Fellow of the Higher Education Academy, UK; Fellow of the Institution of Engineering and Technology, Energy Institute, UK; the Chartered Institution of Building Services Engineers, UK; the Institution of Mechanical Engineers, UK; the Royal Society of Arts, UK, The African Academy of Sciences, and Chartered Institute of Educational Assessors, UK. He is also a senior member of the IEEE.